

# Precise predictions for Higgs production at $e^+e^-$ colliders and Numerical calculation of one-loop integrals \*

M. M. WEBER

Dipartimento di Fisica Teorica, Università di Torino,  
Via Giuria 1, 10125 Torino, Italy

## Abstract

Some of the most interesting Higgs-production processes at future  $e^+e^-$  colliders are of the type  $e^+e^- \rightarrow f\bar{f}H$ . We present a calculation of the complete  $\mathcal{O}(\alpha)$  corrections to these processes in the Standard Model for final-state neutrinos and top quarks. Initial-state radiation beyond  $\mathcal{O}(\alpha)$  at the leading-logarithmic level as well as QCD corrections are also included. The electroweak corrections turn out to be sizable and reach the order of  $\pm 10\%$  and will thus be an important part of precise theoretical predictions for future  $e^+e^-$  colliders.

Furthermore, an overview is given of a technique for a fast and reliable numerical calculation of multi-leg one-loop integrals. The method is numerically stable also for exceptional momentum configurations and easily allows the introduction of complex masses and the calculation of higher orders in the expansion around  $D = 4$ .

## 1 Introduction

One of the main future tasks in particle physics will be the investigation of the mechanism of electroweak symmetry breaking in general and the discovery of the Higgs boson and the determination of its properties in particular. Since the Higgs-boson mass is expected to be in the range from the lower experimental bound of 114.4 GeV up to 1 TeV, with a light Higgs mass (below  $\sim 200$  GeV) favoured by electroweak precision data, the LHC will be able to discover it in the full mass range, provided it exists and has no exotic properties. However, for the complete determination of its profile, including its couplings to fermions and gauge bosons, experiments in the clean environment of an  $e^+e^-$  linear collider are indispensable.

Here we concentrate on the associated production of a Higgs boson together with a pair of neutrinos or top quarks in  $e^+e^-$  annihilation, which are among the most interesting Higgs-boson production processes at future  $e^+e^-$  linear colliders.

---

\*Talk given at the final meeting of the European Network "Physics at Colliders", Montpellier, September 26-27, 2004.

The calculation of the radiative corrections to these processes is presented in the next two sections.

The last section gives a sketch of a technique for a fast and reliable numerical calculation of multi-leg one-loop integrals and describes an implementation of the method in Mathematica and C++.

## 2 The process $e^+e^- \rightarrow \nu\bar{\nu}H$

At  $e^+e^-$  colliders the two main Higgs production processes are the Higgs-strahlung and W-boson-fusion processes. In the Higgs-strahlung process the Higgs boson is radiated off a Z boson, with the corresponding cross section rising sharply at the threshold, located at a centre-of-mass (CM) energy of  $\sqrt{s} = M_Z + M_H$ , to a maximum a few tens of GeV above the threshold energy and then falling off as  $1/s$ . In the W-boson-fusion process the Higgs boson is produced via fusion of two W bosons, each emitted from an incoming electron/positron. The corresponding cross section grows as  $\ln s$  and thus is the dominant production mechanism at large energies. Both production mechanisms appear in the process  $e^+e^- \rightarrow \nu_l\bar{\nu}_lH$ , with  $l = e, \mu, \text{ or } \tau$ , though the W-boson-fusion process is only present for  $l = e$ .

For the process  $e^+e^- \rightarrow ZH$  the  $\mathcal{O}(\alpha)$  electroweak radiative corrections have been calculated many years ago in Ref. [1]. Furthermore a Monte Carlo algorithm for the calculation of the real photonic corrections to this process was described in Ref. [2]. For the full process  $e^+e^- \rightarrow \nu\bar{\nu}H$  there has been a lot of activity regarding the electroweak corrections recently. Within the Minimal Supersymmetric Standard Model (MSSM) the fermion and sfermion loop contributions have been evaluated in Refs. [3, 4]. Analytical results for the one-loop corrections in the SM have been obtained in Ref. [5], though no numerical results have been given there. Finally, calculations of the complete  $\mathcal{O}(\alpha)$  electroweak corrections to  $e^+e^- \rightarrow \nu\bar{\nu}H$  in the SM have been performed in Refs. [6, 7]. Very recently also results on corrections to the Z-boson-fusion process  $e^+e^- \rightarrow e^+e^-H$  have been presented in Ref. [8].

### 2.1 Computational framework

The calculation of the one-loop diagrams has been carried out in the 't Hooft–Feynman gauge using standard techniques. The renormalization is carried out in the on-shell renormalization scheme, as e.g. described in Ref. [9]. The electron mass  $m_e$  is neglected whenever possible.

The calculation of the Feynman diagrams has been performed in two completely independent ways, leading to two independent computer codes for the numerical evaluation. Both calculations are based on the methods described in Ref. [9]. Apart from the 5-point functions the tensor coefficients of the one-loop integrals are recursively reduced to scalar integrals with the Passarino–Veltman algorithm [10] at the numerical level. The scalar integrals are evaluated using the

methods and results of Refs. [9, 11], where ultraviolet divergences are regulated dimensionally and IR divergences with an infinitesimal photon mass. The 5-point functions are reduced to 4-point functions following Ref. [12], where a method for a direct reduction is described that avoids leading inverse Gram determinants which potentially cause numerical instabilities. As a check of gauge independence the calculation of the virtual corrections has been repeated using the background-field method [13].

The results of the two different codes, and also those obtained within the conventional and background-field formalism, are in good numerical agreement (typically within at least 12 digits for non-exceptional phase-space points).

We use two different schemes for the inclusion of the finite Z-boson decay width. In the *fixed-width scheme*, each resonant Z-boson propagator  $1/(s_{\nu\bar{\nu}} - M_Z^2)$ , where  $s_{\nu\bar{\nu}}$  is the invariant mass of the neutrino–antineutrino pair, is replaced by  $1/(s_{\nu\bar{\nu}} - M_Z^2 + iM_Z\Gamma_Z)$ , while non-resonant contributions are kept untouched. This potentially violates gauge invariance, because the resonant part of the amplitude alone is not gauge invariant. As a second option, we applied a *factorization scheme* where the full (gauge-invariant) ZH-production amplitude with zero Z-boson width is rescaled by a factor  $(s_{\nu\bar{\nu}} - M_Z^2)/(s_{\nu\bar{\nu}} - M_Z^2 + iM_Z\Gamma_Z)$ . However in this scheme the non-resonant part of the ZH-amplitude is neglected on resonance. Nevertheless both schemes give the same results for the total cross section within integration errors.

The matrix elements for the real photonic corrections are evaluated using the Weyl–van der Waerden spinor technique as formulated in Ref. [14] and have been successfully checked against the result obtained with the package *Madgraph* [15]. The soft and collinear singularities are treated both in the dipole subtraction method following Refs. [16, 17] and in the phase-space slicing method following closely Ref. [18].

The emission of photons collinear to the incoming electrons or positrons leads to corrections that are enhanced by large logarithms of the form  $\ln(m_e^2/s)$ . In order to achieve an accuracy at the few 0.1% level, the corresponding higher-order contributions, i.e. contributions beyond  $\mathcal{O}(\alpha)$ , must be taken into account. These are included in our calculation at the leading-logarithmic level using the structure functions given in Ref. [19] (for the original papers see references therein).

The calculation is done in the so-called  $G_\mu$ -scheme, i.e. we derive the electromagnetic coupling  $\alpha = e^2/(4\pi)$  from the Fermi constant  $G_\mu$  according to  $\alpha_{G_\mu} = \sqrt{2}G_\mu M_W^2 s_w^2/\pi$ . This procedure absorbs the corrections proportional to  $m_t^2/M_W^2$  in the fermion–W-boson couplings and the running of  $\alpha(Q^2)$  from  $Q^2 = 0$  to the electroweak scale. In the relative radiative corrections, we use  $\alpha(0)$  as coupling parameter, which is the correct effective coupling for real photon emission.

The cross section for  $e^+e^- \rightarrow \nu\bar{\nu}H$  is dominated by the WW-fusion diagram, which gets its main contribution from the region of small momentum transfers. Consequently, the corresponding corrections are determined by the  $e\nu_e W$  and

WWH vertex corrections for small invariant  $W$  masses. The correction to the  $e\nu_e W$  vertex and the main contributions to the WWH vertex in the relevant kinematical region are well approximated by  $\Delta r$ . Thus, parametrizing the lowest order in terms of  $G_\mu$  ( $G_\mu$ -scheme) absorbs a large part of the universal corrections. Further universal corrections have been obtained by extracting the leading  $m_t$ -dependent corrections of the WW-contribution in the heavy-top limit in the  $G_\mu$ -scheme. These reproduce the full  $m_t$ -dependent corrections rather well for the WW channel, which is dominated by small momentum transfers. Therefore, we have defined the following improved Born approximation (IBA)

$$d\sigma_{\text{IBA}}^{\text{non-photonic}} = d\sigma_0 - d\sigma_0^{\text{WW}} \frac{5\alpha}{16\pi s_w^2} \frac{m_t^2}{M_W^2}. \quad (1)$$

The corresponding expression for the  $m_t \rightarrow \infty$  limit of the ZH contribution is not included in the definition of the IBA, since it does not give a good description. In the ZH channel  $\sqrt{s}$  is a typical scale for the momentum transfer, which is larger than  $m_t$  in the physically interesting region of  $e^+e^- \rightarrow \nu\bar{\nu}H$ . Finally,  $d\sigma_{\text{IBA}}^{\text{non-photonic}}$  is convoluted with the ISR structure functions to yield the cross section of the full IBA.

The phase-space integration is performed with Monte Carlo techniques in both computer codes. The first code employs a multi-channel Monte Carlo generator similar to the one implemented in *RacoonWW* [17, 20] and *Lusifer* [21], the second one uses the adaptive multi-dimensional integration program VEGAS [22].

## 2.2 Comparison to related work

We have compared our results for the  $\mathcal{O}(\alpha)$  corrections to Ref. [7] and the contributions from closed fermion loops with Refs. [3, 4].

Adapting the input parameters and the parametrization of the lowest-order matrix element to those used by Belanger et al. [7], we reproduced the numbers for the total cross section given in Table 2 of the first paper of Ref. [7]. Note that we switch off the ISR beyond  $\mathcal{O}(\alpha)$  in this comparison. In Table 1 we list for each Higgs-boson mass the results of Ref. [7]<sup>1</sup> together with our results. The numbers in parenthesis indicate the errors in the last digits. We find agreement within  $10^{-4}$  for the total lowest-order cross section and within 0.3% for the corrected cross section. The corrections relative to the lowest-order cross section agree within 0.2%. This is of the order of the statistical error of Ref. [7], which is about 0.1%. Note that Belanger et al. use  $\alpha(0)$  to parametrize the lowest-order cross section. As a consequence their relative corrections are shifted by  $3\Delta r \approx +9\%$  compared to those in the  $G_\mu$ -scheme.

---

<sup>1</sup>According to F. Boudjema, the numbers for the lowest-order cross section in Table 2 of Ref. [7] have integration errors of the order of 0.2%. Table 1 contains updated numbers obtained with increased statistics.

$M_H$ [GeV]	$\sigma_{\text{tree}}$ [fb]	$\sigma$ [fb]	$\delta$ [%]	
150	61.074(7)	60.99(7)	-0.2	Ref. [7]
	61.076(5)	60.80(2)	-0.44(3)	this work
250	21.135(2)	20.63(2)	-2.5	Ref. [7]
	21.134(1)	20.60(1)	-2.53(3)	this work
350	4.6079(5)	4.184(4)	-9.1	Ref. [7]
	4.6077(2)	4.181(1)	-9.27(3)	this work

Table 1: Total cross section in lowest order and including the full  $\mathcal{O}(\alpha)$  corrections and the relative corrections for  $\sqrt{s} = 500$  GeV and various Higgs masses for the input parameter scheme of Ref. [7]

We have also reproduced the  $\cos\theta_H$  and  $E_H$  distributions in Figures 1 and 2 of the first paper of Ref. [7]. We found agreement within the accuracy of these figures.

When considering only fermion-loop corrections, we find agreement with the calculations of Refs. [3, 4], once the appropriate renormalization and input-parameter schemes are adopted. For more details on this comparison we refer to Ref. [6].

### 2.3 Numerical results

The results for the total cross section in lowest order and including the radiative corrections are shown in Figure 1 on the l.h.s. as a function of the CM energy for  $M_H = 150$  GeV. The relative corrections shown on the r.h.s are large ( $\lesssim -20\%$ ) and vary strongly in the ZH-threshold region while they are flat and about  $-10\%$  for energies above 500 GeV. They are always negative because they are dominated by initial-state radiation and the cross section is monotonously rising. Also shown in Figure 1 on the r.h.s are the residual relative corrections normalized to the IBA which are about 1% near the threshold and reach 3–4% at high energies. Although they are systematically smaller than the corrections relative to the lowest order in the  $G_\mu$  scheme, the inclusion of the full  $\mathcal{O}(\alpha)$  corrections is necessary for a precision analysis.

## 3 The process $e^+e^- \rightarrow t\bar{t}H$

We have also investigated the process  $e^+e^- \rightarrow t\bar{t}H$ , which is interesting since it permits a direct access to the top-quark Yukawa coupling  $g_{t\bar{t}H}$ , which is by far the largest Yukawa coupling ( $g_{t\bar{t}H} \approx 0.5$ ) in the SM. This is possible because the process proceeds mainly through Higgs-boson emission off top quarks, while emission from intermediate Z bosons plays only a minor role if the Higgs-boson

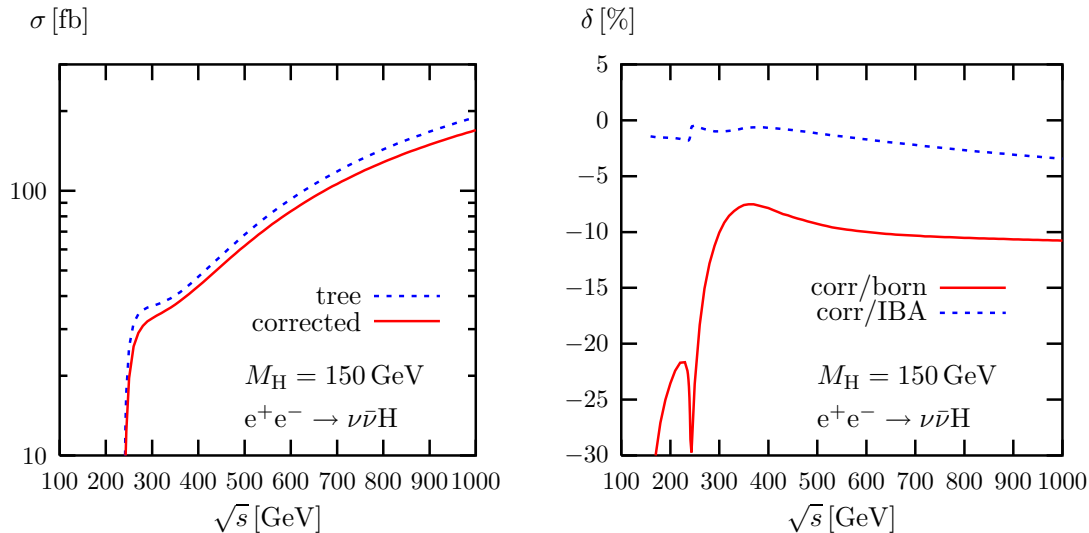


Figure 1: Lowest-order and corrected cross sections (l.h.s.) as well as relative corrections with respect to Born result and improved Born approximation (r.h.s.) in the  $G_\mu$  scheme for a Higgs-boson mass  $M_H = 150$  GeV

mass is not too large, i.e.  $M_H \sim 100\text{--}200$  GeV. For a light Higgs boson with a mass around  $M_H \sim 120$  GeV, a precision of about 5% can be reached at an  $e^+e^-$  linear collider operating at  $\sqrt{s} = 800$  GeV with a luminosity of  $\int L dt \sim 1000 \text{ fb}^{-1}$  [23]. An even better accuracy can be obtained by combining the  $t\bar{t}H$  channel with information from other Higgs-production and decay processes in a combined fit [24].

Within the SM the  $\mathcal{O}(\alpha_s)$  corrections have been calculated for the dominant photon-exchange channel in Ref. [25], while the full set of diagrams has been evaluated in Ref. [26]. The  $\mathcal{O}(\alpha_s)$  corrections to the photon-exchange channel in the MSSM have been considered in Ref. [27]. In Ref. [28] all QCD diagrams have been taken into account, while the SUSY-QCD corrections have been worked out in Ref. [29]. The evaluation of the electroweak  $\mathcal{O}(\alpha)$  corrections in the SM has made considerable progress recently. Results have been presented in Refs. [30, 31, 32], with agreement between Refs. [31, 32] while Ref. [30] shows deviations close to threshold and at high energies.

Our calculation [32] includes the  $\mathcal{O}(\alpha)$  electroweak and the  $\mathcal{O}(\alpha_s)$  QCD corrections. Though the calculation of the virtual corrections for this process is much more involved than for the process  $e^+e^- \rightarrow \nu\bar{\nu}H$ , the same calculational techniques could be used.

$\sqrt{s}$ [GeV]	$\sigma_{\text{tree}}$ [fb]	$\sigma$ [fb]	$\delta$ [%]	
500	$4.8142 \cdot 10^{-4}$	$3.401 \cdot 10^{-4}$	-29.35	Ref. [30]
	$4.8140(8) \cdot 10^{-4}$	$3.168(4) \cdot 10^{-4}$	-34.19(8)	this work
800	1.58	1.63	3.60	Ref. [30]
	1.5749(2)	1.6243(4)	3.14(2)	this work
1000	1.47	1.53	4.47	Ref. [30]
	1.4664(2)	1.5273(4)	4.15(2)	this work
2000	0.6270	0.6297	0.43	Ref. [30]
	0.6269(1)	0.6526(3)	4.11(5)	this work

Table 2: Total cross section in lowest order and including the full electroweak  $\mathcal{O}(\alpha)$  corrections as well as the relative corrections for  $M_{\text{H}} = 150$  GeV and various CM energies for the input-parameter scheme of Ref. [30]. The statistical errors of Ref. [30] are estimated by the authors to be below 1%

### 3.1 Comparison to related work

The results on the QCD corrections have been reproduced with the (publically available) computer code based on the calculation of Ref. [26]. We found agreement within the statistical integration errors.

For a comparison of the electroweak  $\mathcal{O}(\alpha)$  corrections with the results of Ref. [30] we changed our input parameters to the ones quoted there and switched to the  $\alpha(0)$ -scheme. In Table 2 we compare some representative numbers<sup>2</sup> from the calculation of Ref. [30] with the corresponding results from our Monte Carlo generator. The numbers in parentheses give the errors in the last digits of our calculation. The tree-level cross sections coincide within 0.03%. Most of the numbers for the one-loop corrected cross sections agree within 1–2%, i.e. roughly within the estimated error of Ref. [30]. However, for the corrected cross sections at  $\sqrt{s} = 2$  TeV, i.e. at high energies, and the one very close to threshold, i.e. for  $\sqrt{s} = 500$  GeV and  $M_{\text{H}} = 150$  GeV, we find differences of 4% and 7%, respectively. The same holds for the relative corrections. Ours are larger by about 4% at  $\sqrt{s} = 2$  TeV and smaller by about 5% for the selected cross section close to threshold.

Finally, we have also compared the electroweak  $\mathcal{O}(\alpha)$  corrections with Ref. [31], where the  $\alpha(0)$ -scheme has been used. In Table 3 we list the results of Table 2 of Ref. [31] for  $M_{\text{H}} = 120$  GeV together with the corresponding results from our Monte Carlo generator. Again the numbers in parentheses give the errors in the last digits. We reproduce the results for the lowest-order cross section within the

<sup>2</sup>These numbers were kindly provided to us by Zhang Ren-You and You Yu quoting a statistical error below 1%.

$\sqrt{s}$ [GeV]	$\sigma_{\text{tree}}$ [fb]	$\sigma$ [fb]	$\delta$ [%]	
600	1.7293(3)	1.738(2)	0.5	Ref. [31]
	1.7292(2)	1.7368(6)	0.44(3)	this work
800	2.2724(5)	2.362(4)	3.9	Ref. [31]
	2.2723(3)	2.3599(6)	3.86(2)	this work
1000	1.9273(5)	2.027(4)	5.2	Ref. [31]
	1.9271(3)	2.0252(5)	5.09(2)	this work

Table 3: Total cross section in lowest order and including the full electroweak  $\mathcal{O}(\alpha)$  corrections as well as the relative corrections for  $M_{\text{H}} = 120$  GeV and various CM energies for the input-parameter scheme of Ref. [31].

integration errors, which are about  $2\text{--}3 \times 10^{-4}$ . The results for the cross section including electroweak corrections as well as the relative corrections coincide to better than 0.1% which is of the order of the integration error of the results of Ref. [31].

### 3.2 Numerical results

Results for the total cross section in lowest order and the corrected cross section including both the electroweak and QCD corrections are shown in Figure 2 on the l.h.s. Away from the kinematic threshold at  $\sqrt{s} = 2m_t + M_{\text{H}}$  the size of the cross section is typically a few fb, with a maximum at about 800 GeV. On the r.h.s. of Figure 2 the relative corrections are shown. The QCD corrections are large and positive close to threshold where soft-gluon exchange in the  $t\bar{t}$  system leads to a Coulomb-like singularity. For larger energies the QCD corrections decrease, eventually turn negative and reach about  $-8\%$  at an energy of  $\sqrt{s} = 1.5$  TeV. The electroweak corrections are about  $-10\%$  and vary only weakly with energy away from the threshold region, and are thus of a comparable size as the QCD corrections. Close to threshold they reach about  $-20\%$  due to the large ISR QED corrections in this region. The behaviour of the combined electroweak and QCD corrections is dominated by the Coulomb-like singularity close to threshold while turning negative and reaching about  $-15\%$  at high energies.

Summarizing, for both of the processes  $e^+e^- \rightarrow \nu\bar{\nu}H$  and  $e^+e^- \rightarrow t\bar{t}H$  the  $\mathcal{O}(\alpha)$  corrections are sizeable and typically of the order  $\pm 10\%$ . They will thus be an important ingredient of precise theoretical predictions for future  $e^+e^-$  colliders. Our results agree with the ones of an independent calculation within the integration errors, which are around 0.1–0.2%. Moreover, these calculations show that techniques for the calculation of one-loop corrections to  $2 \rightarrow 3$  processes are available and work well in practical applications.



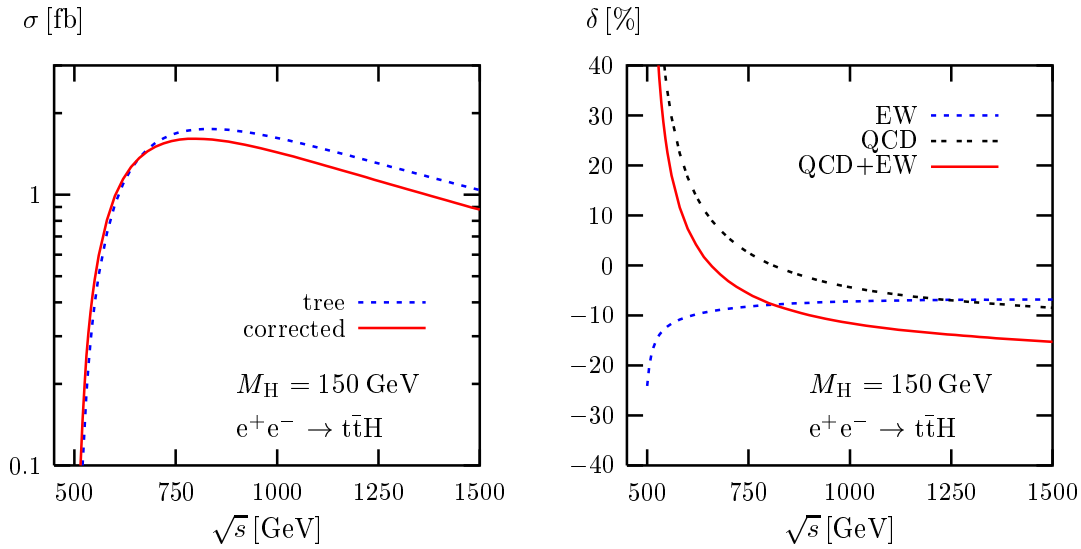


Figure 2: Lowest-order and corrected cross sections (l.h.s.) as well as relative corrections (r.h.s.) in the  $G_\mu$  scheme for a Higgs-boson mass  $M_H = 150$  GeV

## 4 Numerical calculation of one-loop integrals

In this section we present a technique for a fast and reliable numerical calculation of multi-leg one-loop integrals and describe an implementation in Mathematica/C++. The method is numerically stable also for exceptional momentum configurations and easily allows the introduction of complex masses and the calculation of higher orders in the expansion around  $D = 4$ .

Using the conventional analytic approach of Ref. [11] all scalar loop integrals can be expressed in terms of dilogarithms and logarithms. Furthermore, using the reduction algorithm of Ref. [10] all tensor loop integrals, i.e. integrals containing loop momenta in the numerator, can be expressed in terms of scalar integrals. Therefore, a full analytic solution for one-loop integrals exists. However this approach has a number of drawbacks. First of all, with an increasing number of external legs the number of dilogarithms in the analytic expression of a scalar integral increases rapidly. This can lead to cancellations for multi-leg integrals in certain kinematic regions [33]. Furthermore the tensor reduction of Ref. [10] introduces inverse Gram determinants. These can vanish at the phase space boundary even though the tensor coefficients themselves are regular in this region. There are thus cancellations among terms in the numerator that can lead to numerical instabilities. Unstable particles are also an important issue in multi-leg loop calculations, since they appear as virtual particles in the diagrams. One way of dealing with them is the introduction of complex masses for the unstable particles. This requires the evaluation of loop integrals with complex masses which is cumbersome in analytic calculations. Finally, within dimensional regularization the evaluation

of the loop-by-loop contribution to a 2-loop calculation makes it necessary to expand the one-loop integrals beyond the constant term in the expansion around  $D = 4$ . An analytic calculation of these higher-order terms is rather complicated

It seems therefore worthwhile to explore alternative numerical approaches to the evaluation of one-loop tensor and scalar integrals. The strategy adopted here is described in detail in Ref. [34]. It is based on the Bernstein-Tkachov theorem [35] which can be used to rewrite one-loop integrals in Feynman-parametric representation in a form better suited for numerical evaluation. The general method is outlined in the next section and a description of an implementation in Mathematica and C++ is given in the last section.

#### 4.1 Description of the method

Within dimensional regularization in  $D = 4 - 2\epsilon$  dimensions any scalar one-loop integral can be expressed as an integration over Feynman parameters

$$\begin{aligned} I_N^D &= \frac{(2\pi\mu)^{4-D}}{i\pi^2} \int d^D q \frac{1}{[q^2 - m_1^2][(q + p_1)^2 - m_2^2] \cdots [(q + p_{N-1})^2 - m_N^2]} \\ &= (4\pi\mu^2)^\epsilon \Gamma(N - 2 + \epsilon) (-1)^N \int dS_{N-1} V(x_i)^{-(N-2+\epsilon)} \end{aligned} \quad (2)$$

where the integration over Feynman parameters is defined as

$$\int dS_n = \int_0^1 dx_1 \int_0^{x_1} dx_2 \cdots \int_0^{x_{n-1}} dx_n$$

and  $V$  is a quadratic form in the  $N - 1$  Feynman parameters  $x_i$

$$V(x) = x^T H x + 2K^T x + L - i\delta.$$

The coefficients  $H$ ,  $K$  and  $L$  of  $V$  are given in terms of the momenta  $p_i$  and the masses  $m_i$ . Note that we use dimensional regularization not only for ultraviolet but also for infrared (IR) and collinear singularities.

In general the quadratic form  $V$  can vanish within the integration region, though the zero's are shifted into the complex plane by the small imaginary part  $i\delta$ . Since the limit  $\delta \rightarrow 0$  has to be taken in the end, the form given above is not suited for a direct numerical integration.

Instead, the integral can be rewritten before attempting a numerical evaluation using the Bernstein-Tkachov theorem [35]. Applied to the case of one-loop integrals it states that for any quadratic form  $V(x)$  raised to any real power  $\beta$

$$\left[ 1 - \frac{(x - X)_i \partial_i}{2(1 + \beta)} \right] V^{1+\beta}(x_i) = B \cdot V^\beta(x_i), \quad (3)$$

where  $X = -K^T H^{-1}$ ,  $B = L - K^T H^{-1} K$  and  $\partial_i = \partial/\partial x_i$ . Inserting this relation into a Feynman-parameter integral and integrating by parts one obtains

$$\int dS_n V^\beta = \frac{1}{2B(1+\beta)} \left[ (2+n+2\beta) \int dS_n V^{1+\beta} - \int dS_{n-1} \sum_{i=0}^n \chi_i V_i^{1+\beta} \right] \quad (4)$$

where  $\chi_i = X_i - X_{i+1}$  with  $X_0 = 1$  and  $X_{n+1} = 0$  and

$$V_i(x_1, \dots, x_{n-1}) = \begin{cases} V(1, x_1, \dots, x_{n-1}) & \text{for } i = 0 \\ V(x_1, \dots, x_i, x_i, \dots, x_{n-1}) & \text{for } 0 < i < n \\ V(x_1, \dots, x_{n-1}, 0) & \text{for } i = n \end{cases}$$

Applied to the one-loop integral (2) the first term inside brackets in (4) corresponds to the  $N$ -point integral in  $D + 2$  dimensions, while the last term is a sum over  $(N - 1)$ -point integrals in  $D$  dimensions obtained by pinching one propagator.

Recursive application of (4) allows to express any scalar one-loop integral as a linear combination of terms of the form  $\int dS_k V(x_i)^{m-\epsilon}$  with any integer  $m \geq 0$ . A Taylor expansion up to  $\mathcal{O}(\epsilon^a)$  will then result in terms of the form  $\int dS_k V^m \cdot \log^{1+a} V$ . For  $m = 0$  the integrand still contains an integrable (logarithmic) singularity while it is smooth for  $m > 0$ . Although larger values of  $m$  will lead to smoother integrands, the expressions also grow larger due to the repeated application of the BT identity (4). The optimal choice for  $m$  depends on the chosen numerical integration routine and its ability to deal with integrable singularities. Note that the calculation of higher orders of the  $\epsilon$  expansion is straightforward in this approach. Furthermore complex masses can also be introduced easily.

If the integral is infrared or collinear divergent, the repeated application of the BT-identity (4) will eventually result in divergent 3-point integrals. For these  $B = 0$  and using a modified identity the singularities are automatically extracted as poles in  $\epsilon$ .

In the case of tensor integrals the parametric representation of the integral contains in general Feynman parameters in the numerator. The procedure outlined above can also be applied in this case so that no separate reduction to scalar integrals is needed. Furthermore, no inverse Gram determinants are introduced using this approach, making it numerically reliable also for exceptional kinematic configurations.

## 4.2 Implementation

The method outlined above has been implemented in Mathematica and C++ with an emphasis on the full automatization of the whole procedure. The user only has to supply the algebraic values of the Lorentz invariants calculated from the external momenta and the internal masses of the integral. As a result a set of

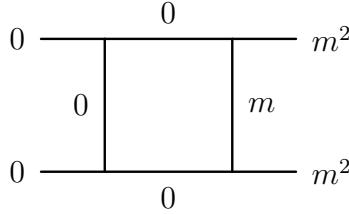


Figure 3: Box-diagram for heavy quark pair production.

C++ routines with a simple interface is generated. These can then be used for a numerical evaluation.

The implementation first generates the parametric representation for the tensor coefficients for a given integral up to the maximum desired tensor rank. The tensor coefficients are defined according to the conventions of Ref. [9]. In the next step consecutive applications of the BT-identities raise the powers of the quadratic forms. IR and collinear singularities show up as poles in  $\epsilon$  during this procedure. Then the expansion in  $\epsilon$  is performed. The power in  $\epsilon$  up to which the integrals are expanded can be chosen by the user. The results of this last algebraic step are a number of Feynman-parameter integrals of different dimensions and in some cases additional constant terms. Each of the integrands is a vector with components corresponding to the tensor coefficients and the components themselves are truncated power series in  $\epsilon$ .

The last step is the generation of C++ routines for the calculation of the various integrands. Furthermore, a driver routine is generated that performs the necessary initializations, calls the numerical integration code and constructs the results for the tensor coefficients from the results of the numerical integrations. This driver routine is the only part of the code the user interacts with directly. It needs only the values for the Lorentz invariants and masses as input and returns the coefficients of the  $\epsilon$  expansion of the tensor coefficients.

As an example we consider the integral shown in Figure 3, which is both IR and collinear divergent. It has been evaluated up to the constant term in the context of the calculation of the next-to-leading order QCD corrections to heavy quark pair production at hadron colliders [36]. Recently also the  $\mathcal{O}(\epsilon)$  coefficient has been calculated analytically in Ref. [37]. Using our numerical program we obtain for  $s = -t = (500 \text{ GeV})^2$  and  $m = 175 \text{ GeV}$

$$\begin{aligned}
 D_0 = & \epsilon^{-2} \cdot (-2.85078 \cdot 10^{-11} + i \cdot 0) \\
 & + \epsilon^{-1} \cdot ( 3.87554(7) \cdot 10^{-10} - i \cdot 4.47800 \cdot 10^{-11}) \\
 & + 1 \cdot (-2.49772(5) \cdot 10^{-9} + i \cdot 6.6096(3) \cdot 10^{-10}) \\
 & + \epsilon^1 \cdot ( 9.9934(2) \cdot 10^{-9} - i \cdot 4.4041(2) \cdot 10^{-9}) \\
 & + \epsilon^2 \cdot (-2.78060(4) \cdot 10^{-8} + i \cdot 1.81859(4) \cdot 10^{-8})
 \end{aligned}$$

$$\begin{aligned}
D_{\mu\nu} = g_{\mu\nu} [ & 1 \cdot (-4.59(4) \cdot 10^{-7} - i \cdot 5.019(5) \cdot 10^{-6}) \\
& + \epsilon^1 \cdot (+1.228(2) \cdot 10^{-5} + i \cdot 4.810(2) \cdot 10^{-8}) \\
& + \epsilon^2 \cdot (-6.697(6) \cdot 10^{-5} - i \cdot 2.259(1) \cdot 10^{-4})] \\
& + \dots
\end{aligned}$$

where numerical integration errors in the last digit are given in parentheses. These results agree with the analytical results within integration errors.

Our implementation is currently capable of handling all triangle integrals up to tensor rank 3 and all box integrals up to rank 4 including IR and collinear divergent integrals. All of these can be calculated up to  $\mathcal{O}(\epsilon^2)$ . A comparison of the finite part and the IR pole with the results of the LoopTools integral library [38] has shown numerical agreement within integration errors for all tensor coefficients of the 3- and 4-point functions. For the 5- and 6-point functions only the scalar integrals are available so far. The implementation of the remaining tensor coefficients is expected to be finished in the near future.

## Acknowledgements

This work was supported by the Swiss Bundesamt für Bildung und Wissenschaft and by the European Community's Human Potential Programme under contract HPRN-CT-2000-00149 Physics at Colliders.

## References

- [1] J. Fleischer and F. Jegerlehner, Nucl. Phys. B **216** (1983) 469; B. A. Kniehl, Z. Phys. C **55** (1992) 605; A. Denner, J. Küblbeck, R. Mertig and M. Böhm, Z. Phys. C **56** (1992) 261.
- [2] F. A. Berends and R. Kleiss, Nucl. Phys. B **260** (1985) 32.
- [3] H. Eberl, W. Majerotto and V. C. Spanos, Phys. Lett. B **538** (2002) 353 [hep-ph/0204280], Nucl. Phys. B **657** (2003) 378 [hep-ph/0210038], and hep-ph/0210330.
- [4] T. Hahn, S. Heinemeyer and G. Weiglein, Nucl. Phys. B **652** (2003) 229 [hep-ph/0211204] and Nucl. Phys. Proc. Suppl. **116** (2003) 336 [hep-ph/0211384].
- [5] F. Jegerlehner and O. Tarasov, Nucl. Phys. Proc. Suppl. **116** (2003) 83 [hep-ph/0212004].
- [6] A. Denner, S. Dittmaier, M. Roth and M. M. Weber, Phys. Lett. B **560** (2003) 196 [hep-ph/0301189] and Nucl. Phys. B **660** (2003) 289 [hep-ph/0302198].

- [7] G. Belanger *et al.*, Phys. Lett. B **559** (2003) 252 [hep-ph/0212261] and Nucl. Phys. Proc. Suppl. **116** (2003) 353 [hep-ph/0211268].
- [8] F. Boudjema *et al.*, hep-ph/0404098.
- [9] A. Denner, Fortsch. Phys. **41** (1993) 307.
- [10] G. Passarino and M. Veltman, Nucl. Phys. B **160** (1979) 151.
- [11] G. 't Hooft and M. Veltman, Nucl. Phys. B **153** (1979) 365. W. Beenakker and A. Denner, Nucl. Phys. B **338** (1990) 349.
- [12] A. Denner and S. Dittmaier, Nucl. Phys. B **658** (2003) 175 [hep-ph/0212259].
- [13] A. Denner, S. Dittmaier and G. Weiglein, Nucl. Phys. B **440** (1995) 95 [hep-ph/9410338].
- [14] S. Dittmaier, Phys. Rev. D **59** (1999) 016007 [hep-ph/9805445].
- [15] T. Stelzer and W. F. Long, Comput. Phys. Commun. **81** (1994) 357 [hep-ph/9401258];  
H. Murayama, I. Watanabe and K. Hagiwara, KEK-91-11.
- [16] S. Dittmaier, Nucl. Phys. B **565** (2000) 69 [hep-ph/9904440].
- [17] M. Roth, PhD thesis, ETH Zürich No. 13363 (1999), hep-ph/0008033.
- [18] M. Böhm and S. Dittmaier, Nucl. Phys. B **409** (1993) 3 and Nucl. Phys. B **412** (1994) 39.
- [19] W. Beenakker *et al.*, in *Physics at LEP2*, eds. G. Altarelli, T. Sjöstrand and F. Zwirner (CERN 96-01, Geneva, 1996), Vol. 1, p. 79 [hep-ph/9602351].
- [20] A. Denner, S. Dittmaier, M. Roth and D. Wackerath, Nucl. Phys. B **560** (1999) 33 [hep-ph/9904472].
- [21] S. Dittmaier and M. Roth, Nucl. Phys. B **642** (2002) 307 [hep-ph/0206070].
- [22] G. P. Lepage, J. Comput. Phys. **27** (1978) 192 and CLNS-80/447.
- [23] H. Baer, S. Dawson and L. Reina, Phys. Rev. D **61** (2000) 013002 [hep-ph/9906419].
- [24] M. Battaglia and K. Desch, hep-ph/0101165.
- [25] S. Dawson and L. Reina, Phys. Rev. D **59** (1999) 054012 [hep-ph/9808443].

- [26] S. Dittmaier, M. Krämer, Y. Liao, M. Spira and P. M. Zerwas, Phys. Lett. B **441** (1998) 383 [hep-ph/9808433].
- [27] S. Dawson and L. Reina, Phys. Rev. D **60** (1999) 015003 [hep-ph/9812488].
- [28] S. Dittmaier *et al.*, Phys. Lett. B **478** (2000) 247 [hep-ph/0002035].
- [29] S. Zhu, hep-ph/0212273.
- [30] Y. You *et al.*, Phys. Lett. B **571** (2003) 85 [hep-ph/0306036].
- [31] G. Belanger *et al.*, Phys. Lett. B **571** (2003) 163 [hep-ph/0307029].
- [32] A. Denner, S. Dittmaier, M. Roth and M. M. Weber, Phys. Lett. B **575** (2003) 290 [hep-ph/0307193] and Nucl. Phys. B **680** (2004) 85 [hep-ph/0309274].
- [33] G. J. van Oldenborgh and J. A. M. Vermaseren, Z. Phys. C **46** (1990) 425.
- [34] A. Ferroglia, M. Passera, G. Passarino and S. Uccirati, Nucl. Phys. B **650** (2003) 162 [hep-ph/0209219].
- [35] F. V. Tkachov, Nucl. Instrum. Meth. A **389** (1997) 309 [hep-ph/9609429];  
I. N. Bernstein, Functional Analysis and its Applications **6** (1972) 26.
- [36] W. Beenakker, H. Kuijf, W. L. van Neerven and J. Smith, Phys. Rev. D **40** (1989) 54.
- [37] J. G. Körner, Z. Merebashvili and M. Rogal, hep-ph/0404069.
- [38] T. Hahn and M. Perez-Victoria, Comput. Phys. Commun. **118** (1999) 153 [hep-ph/9807565].